Biomass Conversion and Biorefinery (2024) 14:6333–6345
https://doi.org/10.1007/s13399-022-02942-y

ORIGINAL ARTICLE

Dissociation of acid blue 113 dye from aqueous solutions using activated persulfate by zero iron nanoparticle from green synthesis: the optimization process with RSM-BBD model: mineralization and reaction kinetic study

Peyman Pourali[1,2] · Aylar Behzad[2] · Ali Ahmadfazeli[3] · S. Ahmad Mokhtari[2] · Yousef Rashtbari[2] · Yousef Poureshgh[2]

Received: 15 February 2022 / Revised: 31 May 2022 / Accepted: 8 June 2022 / Published online: 18 June 2022

Abstract

Dyes are one of the major environmental pollutants in the textile industry effluent. The Most of these compounds are toxic, carcinogenic, mutagenic, and biodegradable. In this study, the response surface method was used to determine the removal optimal conditions of acid blue 113 (AB 113) dye in the presence of nanoscale zero-valent iron (nZVI) particles as activators for persulfate (PS) and the mineralization rate of the dye were investigated. The structure and morphology of nZVI nanoparticles were investigated by using FTIR, FESEM, and XRD techniques. The experiments were evaluated based on the Box-Behnken design with five input parameters such as reaction time, pH, catalyst value (nZVI), PS value, and initial concentration of dye at three levels. Finally, the mineralization rate and kinetic studies were investigated to evaluate the oxidation process. The results of physicochemical analysis confirmed the accuracy of nZVI nanoparticle structure. Under optimal conditions, initial concentration of dye was 46 mg/L, pH = 3, reaction time was 50 min, catalyst dose = 0.08 g/L, PS = 0.14 g/L, and the removal rate obtained was 100%. The proposed model (quadratic) was confirmed by high correlation coefficient $R^2_{Adj} = (0.9724)$ and $R^2 = (0.9872)$. The results illustrated that the reaction kinetic conforms to the pseudo-first-order model (0.9985). The present study showed that the radicals obtained from the activation of persulfate using nZVI nanoparticles have a high efficiency in the removal of AB 113 dye. The results indicated that under optimal conditions, the efficiency of TOC for oxidation of acid AB 113 dye was 79.37%.

Keywords Green synthesis · nZVI · Persulfate · Acid blue 113 · RSM-BBD model · Advanced oxidation

1 Introduction

Nowadays, dyes are widely produced in various industrial fields including the textile industry, food industry, leather industry, and pharmaceutical industry [1, 2]. Annually, about 700,000 tons of dyes are produced all over the world, of which 15% of that amount has entered the environment without any treatment process and about 70% of all of them are azo group dyes [3–5]. Meanwhile, acid blue 113 (AB 113) dye is considered one of the most widely used azo dyes in the textile industry due to its high photolytic stability, resistance to microbial degradation, and high strength on fabrics [6, 7]. AB 113 dye has difficultly dissociated in natural environment and has a high stability due to its aromatic rings and azo bond (-N = N-). On the other hand, the dyes of the azo group are known to be carcinogenic and mutagenic agents with toxic metabolites. In recent years, various methods have been proposed and used for the treatment of colored wastewaters. Existing methods for dye removal include aerobic and anaerobic digestion, coagulation, advanced oxidation, combined chemical and biochemical processes, adsorption, and membrane treatment. Each of these methods has different removal efficiencies, advantages, disadvantages,

✉ Yousef Poureshgh
yusef.poureshg@gmail.com

1 Students Research Committee, Faculty of Health, Ardabil University of Medical Sciences, Ardabil, Iran

2 Department of Environmental Health Engineering, School of Health, Ardabil University of Medical Sciences, Ardabil, Iran

3 Department of Environmental Health Engineering, School of Health, Tehran University of Medical Sciences, Tehran, Iran

investment, and operating costs. The oxidation power for removing contaminants in the advanced oxidation process based on the production of hydroxyl free radicals (OH^*) has been high that convert many organic chemical compounds into minerals. These radicals are unstable and highly active, which are produced through chemical or photochemical reactions at the site. Free radicals are strong oxidants that rapidly attack organic matter molecules and separate a hydrogen atom from the structure of organic matter [8–14].

Nowadays, the usage of persulfate as an oxidizing agent is expanding. Persulfate [15] is a non-selective anion, soluble and relatively stable at room temperature, and is the strongest oxidant of the peroxygen family. Its oxidation–reduction potential is 2.1 V and it is stronger than hydrogen peroxide (1.8 V) and permanganate (1.7 V) but is slightly weaker than ozone (2.2 V). In addition, the sulfate radical has more chance for reacting with organic compounds than the hydroxyl radical (20 ns) due to its longer durability (30–40 µs). PS and its resulting sulfate radicals have special and unique properties such as high kinetic velocity, greater stability compared with hydroxyl radicals, and less dependence on natural organic matter, which itself has a greater impact on organic matter [16, 17]. Under atmospheric conditions, the oxidation of PS does not have much effect on organic pollutants, but if heat, light, or certain metal ions are used as catalysts, the reaction of PS will significantly increase. The processes that occurred in the case of the use of PS are given in Eqs. 1 and 2 [18].

$$S_2O_8^{2-} + \text{heat or UV} \rightarrow 2SO_4^{-\bullet} \quad (1)$$

$$S_2O_8^{2-} + \text{Metal ions} \rightarrow Me^{+} + SO_4^{2-} + 2SO_{4-} \quad (2)$$

The advantages of using this oxidizer include high solubility in aqueous environments, non-selective reactivity, relative stability at ambient temperature, reaction with most organic-based contaminants, and chemical stability in aqueous systems [19]. Hydroxyl radical and sulfate radical are both strong oxidants. The produced sulfate radical from PS can destroy a number of radical chain reactions in which organic matter presents [20]. As mentioned, one of the ways of activating PS is using metal ions such as iron and cobalt. Iron is considered to be atoxic, inexpensive, and effective. Reactions that occur in the presence of iron ion include the following reaction [21]. The following reaction shows the chemical activation of PS by an intermediate metal (Eq. 3).

$$S_2O_8^{2-} + Me^{2+} \rightarrow SO_{4\cdot-} + Me^{3+} + SO_{4^{2-}} \quad (3)$$

Among metals, the most application is related to divalent iron (Fe^{2+}), in which the large amounts of requirement, high production of sludge, and consumption of $SO_4^{\bullet-}$ radicals in high concentrations are the main problems of this activator [22]. Due to the problems associated with the usage of this activator, in this study, zero-valent iron nanoparticle (nZVI) was applied, which is able to act as a permanent source of Fe^{2+} and continuously enters iron into the reaction. The reaction of Fe° with PS is shown in the form of the following reactions (Eqs. 4 and 5) [23, 24].

$$Fe^{\circ} + S_2O_8^{2-} \rightarrow Fe^{2+} + 2SO_4^{2-} \quad (4)$$

$$S_2O_8^{2-} + Fe^{2+} \rightarrow SO_4^{\bullet-} + Fe^{3+} + SO_4^{2-} \quad (5)$$

In 2021, Soubh et al. used the optimization process for the removal of methylene blue from aqueous solutions using activated persulfate by nano-scale zero-valent iron (nZVI) which is supported by reduced expanded graphene oxide (rEGO). The highest removal efficiency obtained with pH = 3, activating dose = 1.2 g/L, persulfate concentration of 0.576 g/L, and reaction time of 20 min was 96% [25]. The response surface method (RSM) is a powerful tool for statistical modeling that is performed by applying the least number of experimental experiments according to the experiment design [26]. RSM is based on a nonlinear multivariate model that consists of a design of experiment for providing sufficient and reliable response values and subsequently a mathematical model that has the best fits with the information obtained from the experimental design and determines the optimal value of the independent variables that produce the most or the least response [27–29]. Central points are a method for estimating and evaluating experiments' error and measuring fitting weakness [30]. RSM itself has different types and this statistical method can be used in various ways. One of its types is the Box-Behnken (BBD) method, which is a second-order design based on three-level incomplete factorial designs [31, 32]. This method can estimate the value of the parameters in a second-order model, make the required designs, and calculate the amount of the nonconformance of parameter [15]. The aim of this study was the optimization of AB 113 dye removal in the zero-valent iron nanoparticle/persulfate process (nZVI @PS) by using a statistical model of the response procedure from aqueous environments.

2 Method

2.1 Required chemicals

AB 113 dye was provided as a precursor of colored pollutant from Alvan Sabet Hamedan Company and nZVI nanoparticle was prepared by synthesis in the laboratory. The general characteristics of AB 113 dye are presented in Table 1 [6, 33]. Also, H_2SO_4 and NaOH were prepared from Germany's Merck Company with laboratorial degree of purity to adjust

Table 1 Physicochemical characteristics of AB 113dye

λ_{max}	Molecular structure	Chemical structure	Molecular weight (g/mol)
570	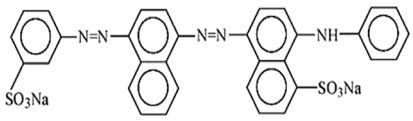	$C_{32}H_{21}N_5Na_2O_6S_2$	681.66

Table 2 Information about the levels and range of studied variables

Variable	Sign	Unit	Levels		
			−1	0	+1
Initial pH of the solution	A	-	3	7	11
The value of nZVI	B	g/L	0.01	0.055	0.1
Persulfate concentration	C	mM	0.01	0.105	0.2
Contact time	D	min	10	35	60
Initial concentration of dye	E	mg/L	25	112.5	200

the pH of the solution containing dye. It should be noted that double-distilled water was used in all stages of the experiments [12].

2.2 Preparation of nZVI nanoparticles by green synthesis method

Grape leaf was used to synthesize nanoparticles by green method. For this purpose, the first 30 g of grape leaf was added to 500 mL of distilled water and then placed on a magnetic stirrer-heater at a speed of 300 rpm for 60 min at 80 °C till the mixing is done. After elapsing mentioned the time, the extraction process was performed from the solution and after cooling, the vacuum pump was filtered by using paper filters. The extract made by iron chloride was mixed with a specific normality in a ratio of 2 to 3. In the next step, the synthesized nanoparticles were dried for 1–2 days at ambient temperature. After this step, the produced nanoparticles were stored for later uses [16, 34, 35].

2.3 Experiment method

Dye stock solution was prepared by dissolving the powder of AB 113 dye in double-distilled water at a concentration of 1000 mg/L. Then, the desired concentrations in mg/L were prepared in a volume of 100 mL of stock solution. The most important effective variables include solution pH, catalyst value (nZVI), PS value, contact time, and initial concentration of dye (Table 2). In this study, the effect of these variables on the performance of dye dissociation by nZVI@PS nanoparticle was investigated. The pH of the solution was adjusted by using 0.1 N sulfuric acid and sodium hydroxide solutions. At all stages, the mixing rate was 250 rpm and all experiments were performed at ambient temperature. At the end of the determined reaction time, the solution was centrifuged by a centrifuge at 3000 rpm for 5 min and prepared for measuring the concentration of residual dye. For ensuring of the results' repetition, each step of the experiment was repeated three times and the average results were reported. The residual concentration of AB 113 dye was determined by the spectrophotometer DR5000 manufactured by the American HACH company at a wavelength of 570 nm [22]. AB 113 dye removal efficiency was determined after the process through Eq. 6 [36–38].

$$\text{Removal efficiency}(\%) = \frac{C_o - C_t}{C_o} \times 100 \quad (6)$$

where C_o and C_t are respectively the initial and final concentrations of AB 113 dye in the solution in mg/L.

2.4 Experiment design based on BBD

Response surface methodology evaluates the existing relationships between clusters of experimental agents by using experimental techniques and then analyzes and presents graphs by investigating the responses based on one or more selected criteria [39, 40]. In this study, solution pH, catalyst dose, amount of persulfate, contact time, and contaminant concentration were selected as independent variables affecting the removal efficiency of AB113. Design Expert 10 software was applied to survey the effect of independent variables on response performance (AB 113 removal efficiency). The design was done by using the Box-Benken Design method. The number of test steps was determined by using Eq. 7 [41–43].

$$N = 2K(K - 1) + C_O \quad (7)$$

where K is the number of factors examined and C_o is the number of repetition steps of the test. After selecting the design, the model equation and its predicted coefficients were determined by the second-order equation (Eq. 8):

$$Y = C_{k0} + \sum_{i=1}^{4} C_{ki}x_i + \sum_{i=1}^{4} C_{kii}x_i^2 + \sum_{i<j=2}^{4} C_{kij}x_i x_j \quad (8)$$

The values of Ck_0, Cki, Ckii, and Ckij are constant, linear, second-order, and regression interaction coefficients, respectively. Xi and Xj are independent coded variables [40, 44]. Statistical analysis was performed to evaluate the accuracy and adequacy of the models by using the analysis of variance (ANOVA) with probability values of Prob ≤ F < 0.05. The adequacy and predictability of the model were tested using the lack of fit criterion, the determination of linear regression coefficient R^2, R^2_{Adjust}, $R^2_{Predicted}$, adequate precision, and residual detection.

2.5 Presentation of second-order polynomial model and ANOVA analysis

According to the Box Behnken scheme, the empirical relationship between input variables and experimental results is represented by a second-order polynomial equation. The resulting equation based on coded factors is:

$$\begin{aligned} Y = {} & +87.15 - 32.49A + 9.6B + 6.4C - 15.3D + 18.32E \\ & -2.47AB - 3.7AC + 6.56AD + 11.46BC - \\ & 1.72BD + 1.35BE + 0.4375CD - 2.01CE - 2.93DE - 21.9A^2 \\ & -17.08B^2 - 16.38C^2 - 15.93D^2 - 18.44E^2 \end{aligned} \quad (9)$$

which in this equation, Y represents the removal rate (%) and A, B, C, D, and E represent pH, nZVI, PS, initial concentration, and reaction time, respectively. The results of the ANOVA analysis in Table 3 show that the proposed model has statistically a significant relationship with linear conditions according to one-way analysis of variance with value of $p \leq 0.001$. Also, A, B, C, D, and E parameters are quite significant interaction of B^2 ($p \leq 0.001$). The value of F for this model has been 48.69, which means that the variance of each variable is significant compared with the error variance, and all the main parameters play an important role as the answer.

With $F = 434.28$ is the most effective factor in the oxidation process of AB 113. In addition, the adjusted correlation coefficient ($R^2_{(adj)}$) is equal to 0.9724 that indicates the high accuracy of the statistical model.

2.6 Analysis tools

For determining the functional groups at the nZVI nanoparticle surface, FTIR analysis was performed by PerkinElmer, Spectrum Two model, in the range of 450–4000 cm^{-1}. X-ray diffraction for the prepared nZVI nanoparticle in the angle range of $2\theta = 10–80°$ was determined by XRD (Philips

Table 3 Analysis of variance of operating parameters in AB 113 oxidation

Source	Sum of squares	df	Mean square	*F*-value	*p*-value	
Model	37,866.68	20	1893.33	48.69	< 0.0001	significant
A-pH	16,888.30	1	16,888.30	434.28	< 0.0001	
B-nZVI	1475.90	1	1475.90	37.95	< 0.0001	
C-PS	656.26	1	656.26	16.88	0.0003	
D-CONC	3747.28	1	3747.28	96.36	< 0.0001	
E-Time	5371.42	1	5371.42	138.13	< 0.0001	
AB	24.45	1	24.45	0.6288	0.4347	
AC	54.69	1	54.69	1.41	0.2460	
AD	172.13	1	172.13	4.43	0.0448	
AE	13.84	1	13.84	0.3559	0.5558	
BC	525.56	1	525.56	13.51	0.0010	
BD	11.76	1	11.76	0.3025	0.5868	
BE	7.26	1	7.26	0.1868	0.6691	
CD	0.7656	1	0.7656	0.0197	0.8895	
CE	16.16	1	16.16	0.4156	0.5246	
DE	34.28	1	34.28	0.8815	0.3561	
A^2	4606.18	1	4606.18	118.45	< 0.0001	
B^2	2800.71	1	2800.71	72.02	< 0.0001	
C^2	2576.38	1	2576.38	66.25	< 0.0001	
D^2	2435.51	1	2435.51	62.63	< 0.0001	
E^2	3263.00	1	3263.00	83.91	< 0.0001	
Residual	1049.97	27	38.89			
Lack of fit	887.84	20	44.39	1.92	0.1924	Not significant
Pure error	162.13	7	23.16			
Cor. total	38,916.65	47				

PNA-analytical diffractometer device). FE-SEM scanning electron microscope at an accelerated voltage of 10 keV was used to determine the surface and morphological characteristics.

3 Results and discussion

3.1 Surveying the structural nature of the nanoparticles

3.1.1 Investigation of nZVI factor groups by using FTIR analysis

One of the common methods used for identifying and analyzing materials is infrared spectroscopy. The results of FTIR nZVI nanoparticle at a frequency of 450–4000 cm^{-1} as illustrated in Fig. 1. The largest peak in the range of 3364 has been shown that is related to the O–H tensile vibrations of the hydrogen bond of polyphenols [45]. Peaks of 1649, 1153, and 1018 are respectively related to the tensile vibrations of C = C alkenes, the tensile vibrations of C–C aromatics, the tensile vibrations of C–O–C carbonyls, and the flexural vibrations of C–H aromatics [45–48]. Peaks at 830 cm^{-1} indicate H-C groups [49, 50]. Peaks at 604 and 535 cm^{-1} indicate the presence of Fe–O groups [51]. Polyphenols act as the main stabilizing agent for nanoparticles, which are found in the range of 3200–3500 cm^{-1} [52, 53]. Bonds of functional groups such as CO–C, C–O, and C = C are derived from heterocyclic compounds and amide bonds are derived from proteins in plant extracts, and the ligands are nanoparticle coating. In addition, the available proteins prevent the formation of clots and help to stabilize the nanoparticles by forming a membrane and cover the metal nanoparticles [54].

3.1.2 Investigation of the structure and nature of nZVI using XRD analysis

The X-ray diffraction pattern (XRD) can be seen in Fig. 2 for nanoparticle in the angle range of 2θ. The XRD diffraction pattern was used to characterize the crystalline phase of nanoparticles and to measure their structural properties. As shown in the figure, the peak of Fe° was determined at angle of $2\theta = 44.67$ [55]. There are some other weak peaks with less intensity at angles of $2\theta = 32$–47-59, which indicate the presence of KCl. Also, the peak at points of $2\Theta = 31$–36-53–63 indicates the presence of NaCl. In the study of Hosseinzadeh et al., impurities such as copper, cadmium, lead, and magnesium were recognized in very small amounts in the composition of nanoparticles used in their study [56]. Also, Lily et al. reported NaCl peaks in XRD test on iron nanoparticles synthesized from plant extract [52].

3.1.3 Morphology surveying of nZVI using FE-SEM analysis

Scanning electron microscopy (FE-SEM) was used to determine the surface and morphological characteristics. The results of nZVI nanoparticle analysis are illustrated in Fig. 3. As shown

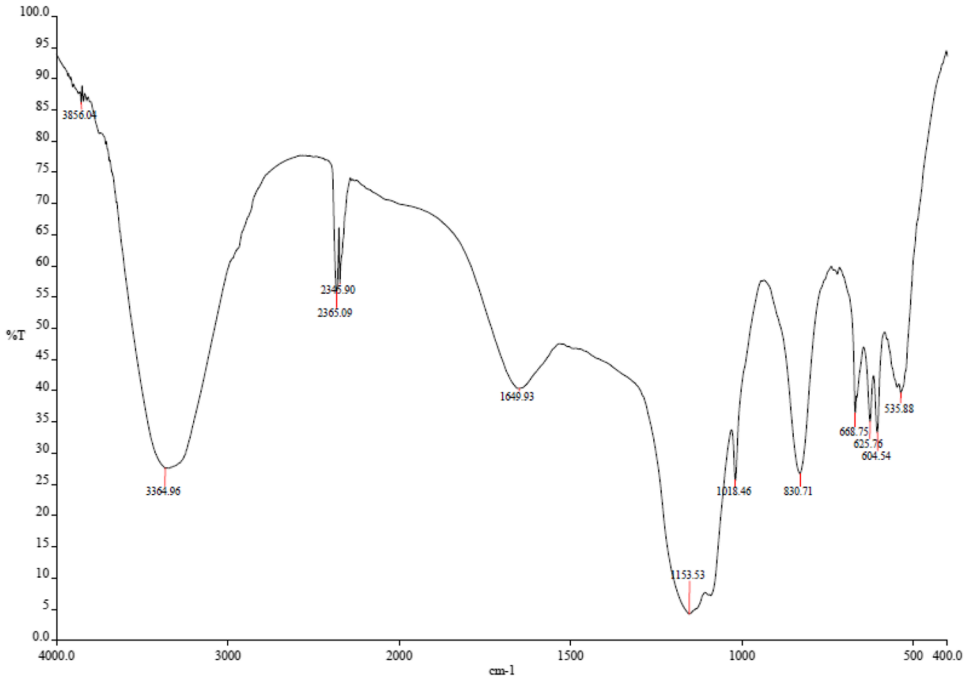

Fig. 1 FTIR spectrum for nZVI

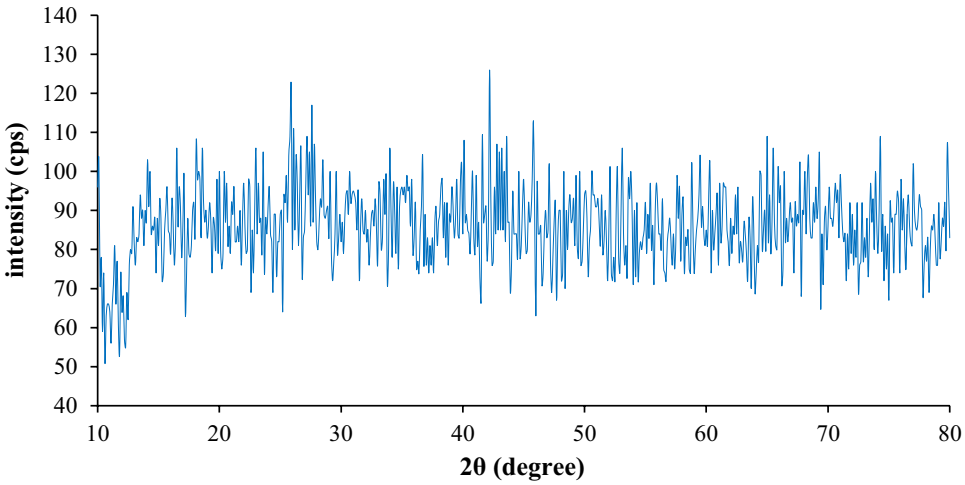

Fig. 2 XRD spectrum for nZVI

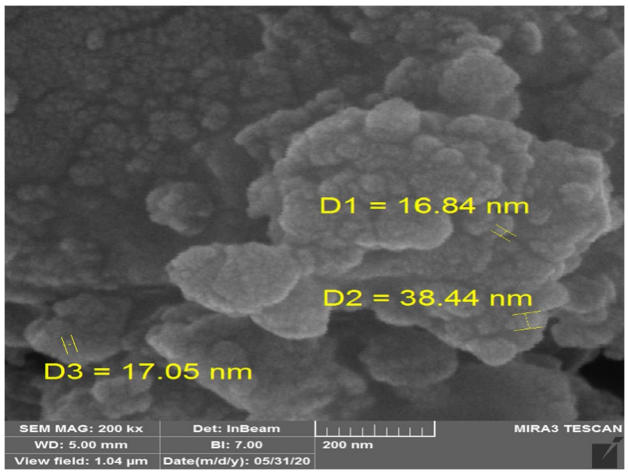

Fig. 3 FE-SEM spectrum for nZVI

in the figure, nZVI particles have a regular morphology and are uniformly, spherically, and homogeneously placed next to each other to form a chain-like structure [57]. The high magnification FE-SEM image shows that the sizes of these nZVI particles range from 15 to 40 nm. Some of nZVI nanoparticles agglomerate together and precipitate during the heating process and indicate the morphology of nZVI particles with a spherical nanosphere size [58].

3.2 The effect of pH on the oxidation efficiency of AB 113 dye

The results of the effect of pH on the rate of dye removal are shown in Fig. 4a. The surveyed pHs in this process were 3, 7, and 11. As it is known, the highest efficiency of the process in the dye removal was related to pH = 3 and was 100%. By increasing the pH of the studied samples, the removal efficiency significantly decreased in which the minimum amount of dye was removed at pH 11. pH and optimal time were respectively determined to be 3 and 50 min. The pH of the solution is one of the most effective and important factors in performing chemical reactions that affect the path and synthetics, the studied contaminant structure, the mechanism of hydroxyl radical production, and the reaction of reactants [59]. In oxidation processes, including electrochemical methods, pH is one of the important items [60]. At alkaline pH due to the sedimentation of iron hydroxide at the surface of nZVI, which leads to occupy the reaction sites and to slow down the reaction by releasing iron ions and electrons. At pH = 3, nZVI dissolves rapidly in the solution, leading to insufficient levels [61]. Also at pHs above 3, the solubility of the residual iron in the solution decreases and the iron becomes colloidal in form. This phenomenon reduces efficiency in turn [62, 63], which is consistent with the results of Qayateri et al. [64].

3.3 Investigation of the effect of persulfate concentration on the oxidation efficiency of AB 113 dyes

The results of the effect of persulfate concentration on the removal of AB 113 dye are shown in Fig. 4b. At this stage of the study, the effect of persulfate anion concentration in the range of 0.01 to 0.2 g/L was evaluated and the optimal dose was obtained 0.14 g/L. The reason of increasing the reaction efficiency by rising PS concentration is the boost in the production of active radicals [65]. Increasing the concentration of PS as the main source of hydroxyl radical production will enhance efficiency.

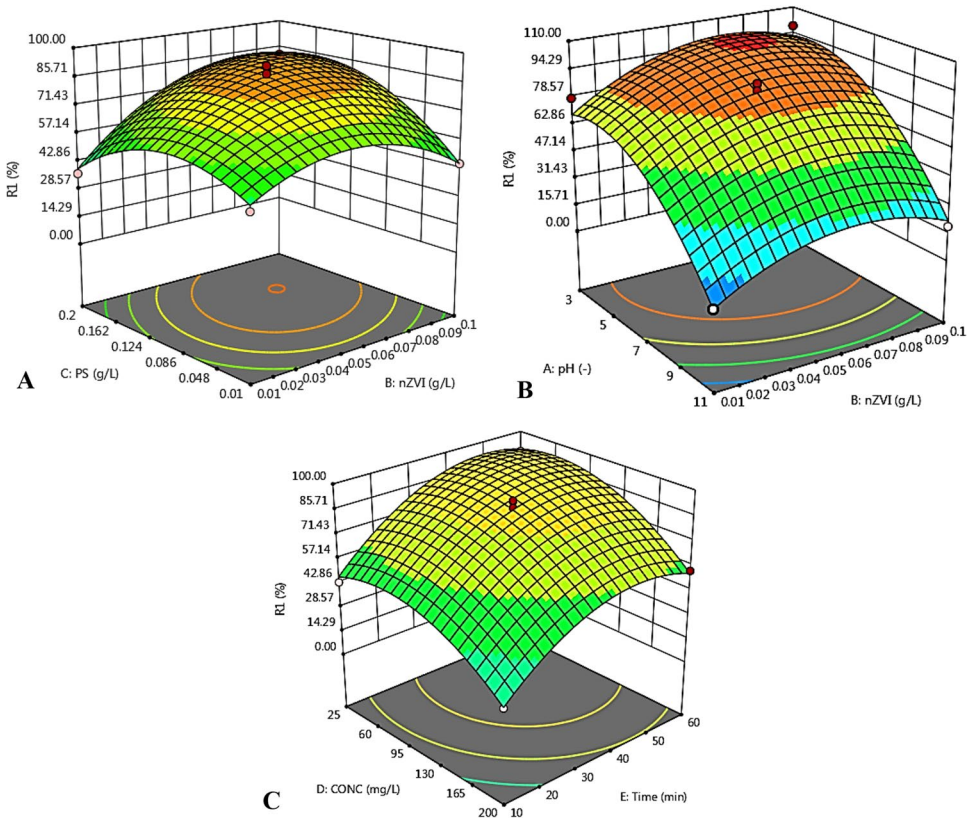

Fig. 4 Overlap diagram of the independent variable effects on AB 113 removal efficiency. **a** PS and nZVI, **b** pH and nZVI; **c** initial dye concentration and reaction time

However, in relation to the consumption concentration of PS, increasing the concentration of this substance to a certain extent not only does not increase the efficiency of the desired contaminant removal, but also has been turned into a factor for abduction and consumption of hydroxyl radicals in aqueous solution, which will reduce the process efficiency [66, 67]. The results of this study agree with the results of the study of Shokouhi et al. [68].

3.4 Surveying the effect of nZVI concentration on the oxidation efficiency of AB 113 dye

To study the effect of nZVI concentration on the degradation of AB 113 dye, nZVI concentration was selected in the range of 0.01–0.1 g/L. As shown in Fig. 4b, the degradation efficiency increased by rising nZVI concentration from 0.01 to 0.1 mg/L and in this study, the optimal concentration of nZVI was 0.08 mg/L. As the amount of nZVI increased, more active surface sites were created to accelerate the initial reaction, leading to more nZVI surface collisions with azo dye molecules to increase AB 113 degradation [61]. nZVI augments the oxidation process due to its large surface area and thus increases the amount of acid blue dye degradation [69].

3.5 The effect of contact time on the oxidation efficiency of AB 113 dye

Figure 4c shows the effect of contact time on the removal efficiency of AB 113 dye. In order to evaluate the optimal contact time, the experiments were performed in the range of 10–60 min. The stirrer speed was 250 rpm. Contact time is one of the most important factors influencing the removal processes. In this process, the highest percentage of AB113 dye removal is related to the reaction time of 50 min, which is describable because of having enough opportunity to produce more free radicals and their contact with dye molecules [70]. Since the addition of electrolysis time leads to the rise in amount of produced hydroxyl radical, therefore, degradation efficiency of AB 113 increases by this process [71]. By adding the contact time, the amount of AB113 dye removal increases, which is consistent with the results of Samarghandi et al. [72].

3.6 The effect of initial concentration of AB 113 dye at equilibrium time on process efficiency

The results of this part of the study about the effect of changes on initial concentration of dye are illustrated in Fig. 4c. Increasing the concentration of AB 113 dye encountered the efficiency of the process with reduction.

In order to evaluate the optimal concentration of AB 113 dye, the experiments were performed in the range of 25–200 mg/L. The optimal concentration of AB 113 dye in the process was 46 mg/L. Due to the fact that the number of produced radicals in different concentrations are different, so the removal efficiency is different too [73]. In most of the studies related to dye oxidation, increasing the concentration of studied contaminants has been associated with decreasing process efficiency. The cause can be attributed to the decrease in the ratio of the produced radical to the concentration of the pollutant and the other cause can be attributed to the increase in the concentration of intermediate substances resulting from the oxidation of the pollutant that tend to consume the radical [74]. The results of this study agree with the results of studies by Seid Mohammadi et al. [59].

3.7 Investigation the accuracy and validity of the proposed model

In order to validate the proposed model, various analyses were performed. The graph of experimental data versus the predicted data by the model of Fig. 5 shows that the values are placed uniformly and compatible with each other along a straight line and have a high correlation [75]. In statistical analysis of the experimental data, checking that the data has a normal distribution is necessary. In the normal distribution, the points related to the data are very close together and are the follower of a straight line that is descending. To determine whether the data is normally distributed or not, the normal probability diagram is shown in Fig. 6. According to the relevant diagram, it is quite obvious that the data related to oxidation reasonably have a normal distribution. Based on the results of Pareto diagram in Fig. 7, it was observed that in the negative effect, pH had the highest efficiency in the removal of AB 113 and the most positive effect on the removal of AB 113 was related to the reaction time. Figure 8 indicates the considered effective variables for oxidation AB 113 including (reaction time, pH, catalyst value (nZVI), PS value, and initial concentration of dye). The selective range of variables, the degree of impact, and the optimal points of each variable can also be seen in this figure.

3.8 Investigation of process kinetics

In all AOP and EOP studies, determining the reaction kinetics is one of the main steps of the study. The study of reaction kinetics is performed to find the oxidation mechanisms of pollutants and the reaction of the model and the better execution of the process. For investigating the reaction kinetics, the first-order reaction model was evaluated under optimal conditions and at different times [76, 77].

$$\frac{\ln c}{c_0} = -k_1 t r_c = \frac{dc}{dt} = k_1 c \tag{10}$$

Based on the indicated kinetic coefficient, the removal rate follows the first-order reaction in this process, in which

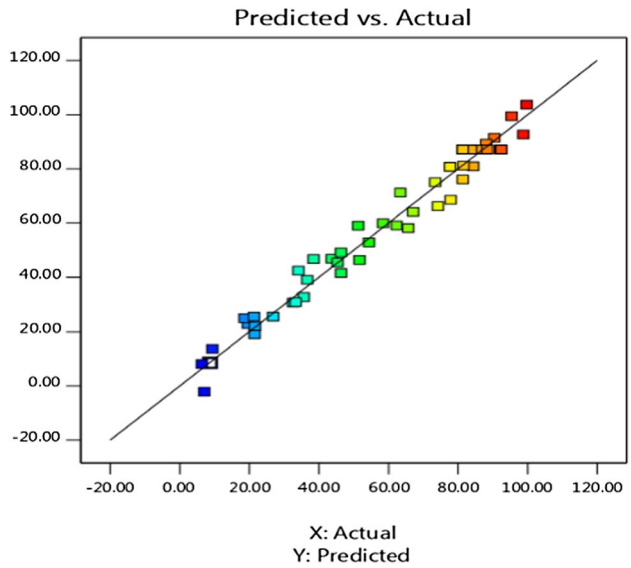

Fig. 5 Fit of experimental data against predicted data

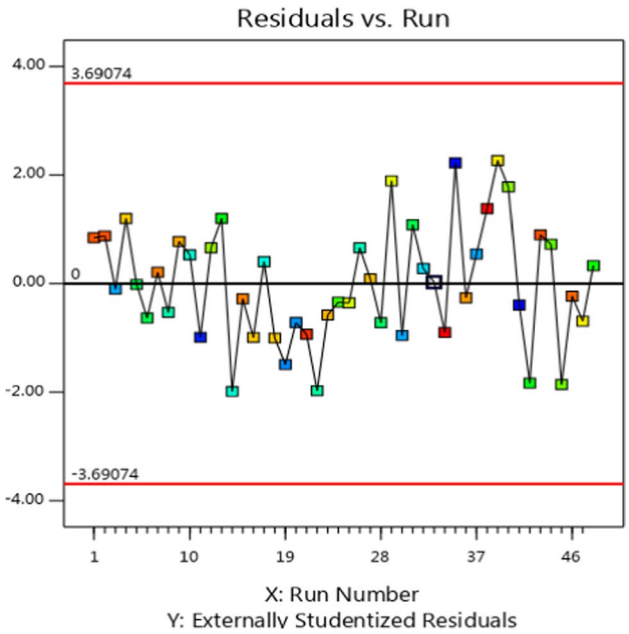

Fig. 6 Normal probability

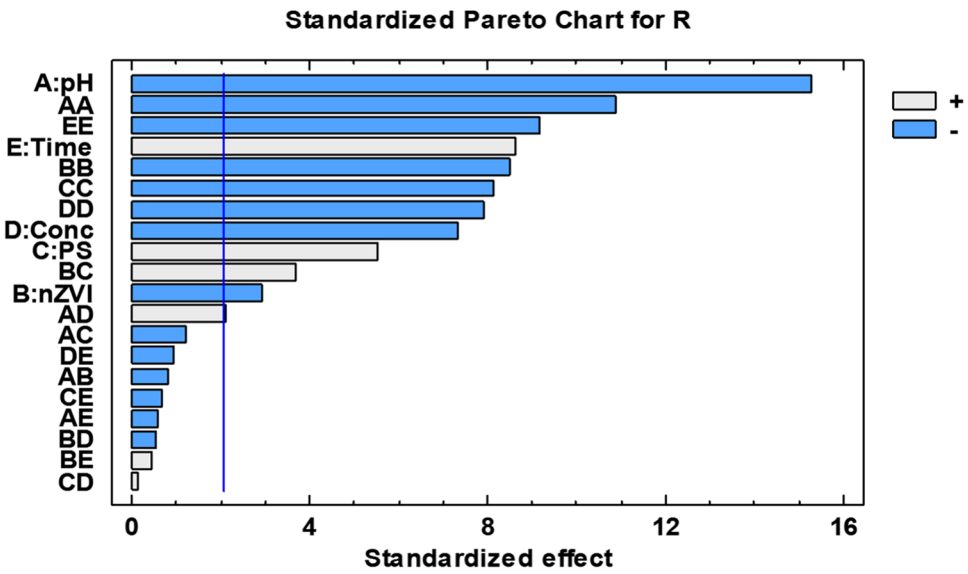

Fig.7 Pareto diagram showing the effect of factors on the removal of AB 113

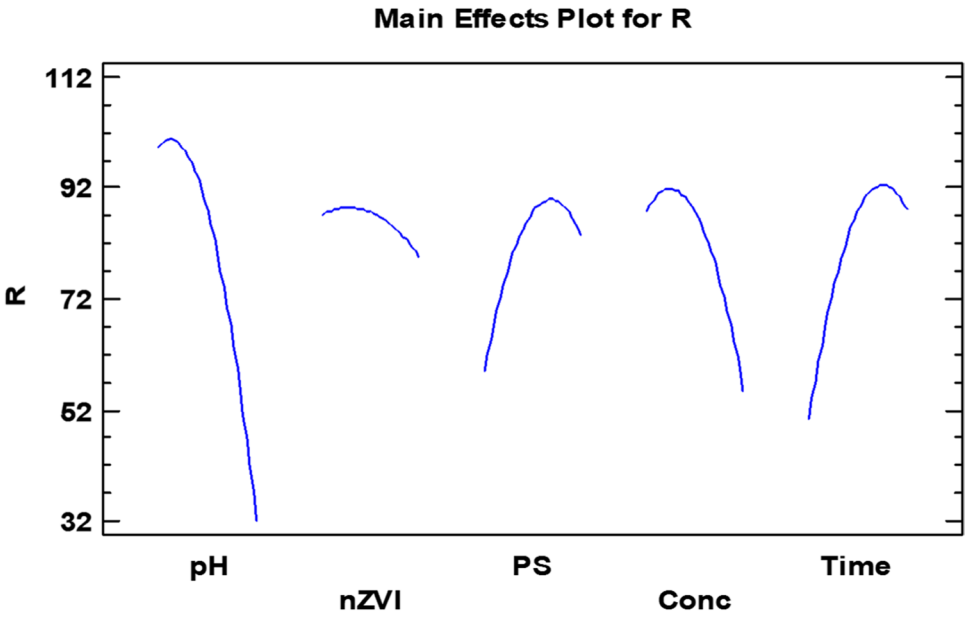

Fig. 8 The effect of the considered initial parameters and their optimal points

the results of study are shown in Fig. 9. Reaction kinetics used to study the rate of chemical reactions. The reaction rate can be indicated by decreasing the concentration of a reactant per unit time or increasing the concentration of a product per unit time [78]. The results of the study are consistent with the results of the study of Dargahi et al. [79].

3.9 TOC analysis

At this stage, all variables were selected and adjusted for the optimal case. The optimal conditions including values of pH = 3, nZVI = 0.08, PS = 0.14, and the concentration of AB 113 = 46 mg/L and reaction time of 50 min were used for this step and the results showed that after 50 min in optimal conditions, TOC efficiency reached to 79.37%. The initial TOC value is equivalent to 640 mg/L, which has reached a concentration of 132 mg/L with a removal efficiency of 79.37% at the end of the reaction time. The reduction of mineralization efficiency compared with dye removal can be observed in the most oxidation processes. This cause can be a result of the production of carbon generator intermediate compounds that are not fully mineralized [80, 81].

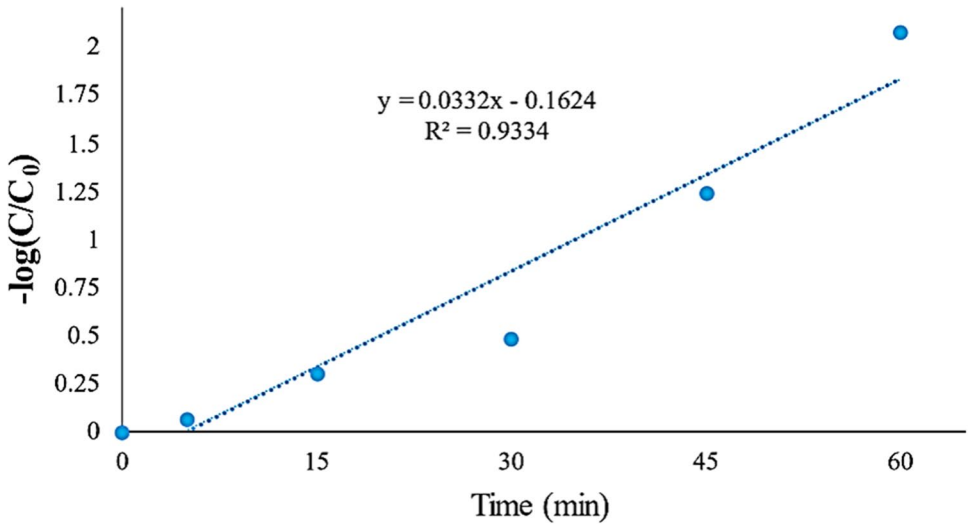

Fig. 9 Reaction kinetic for oxidation of AB 113

3.10 Stability and repeatability of nZVI

An important feature of a heterogeneous catalyst is its reusability and high stability for real-scale applications. In this study, the reusability of the nZVI catalyst was evaluated in four consecutive oxidation cycles under optimal conditions (see Fig. 10). Here, the reusability of the nZVI was evaluated by repeated regeneration via a washing catalyst using 0.1 mol/L NaOH solution and deionized water. As can be seen, under the optimum conditions, the efficiency for AB113 removal was 100% and reached 95.43% after four cycles. These results confirm that the nZVI catalyst has high reusability. However, the slight decrease in the efficiency can be attributed to the change in the physicochemical properties of the catalyst, which will eventually reduce the number of active sites for $fe.^{2+}$ release [82–84]

3.11 Application of nZVI @PS using real samples

Further investigation of the removal of AB113 onto the nZVI @PS was performed by means of the real wastewater samples. The samples were obtained from the Sivan Textile Company in Ardabil. The treatment was subjected to the nZVI @PS under optimized conditions. It should be noted that the samples contained a large variety of other contaminants which could compete with the target contaminants for the adsorption sites. However, the results showed that the nZVI @PS still had significant efficiency of dye removal (81.43%). This observation suggests that the nZVI @PS has a good potential for the removal of dyes in real samples.

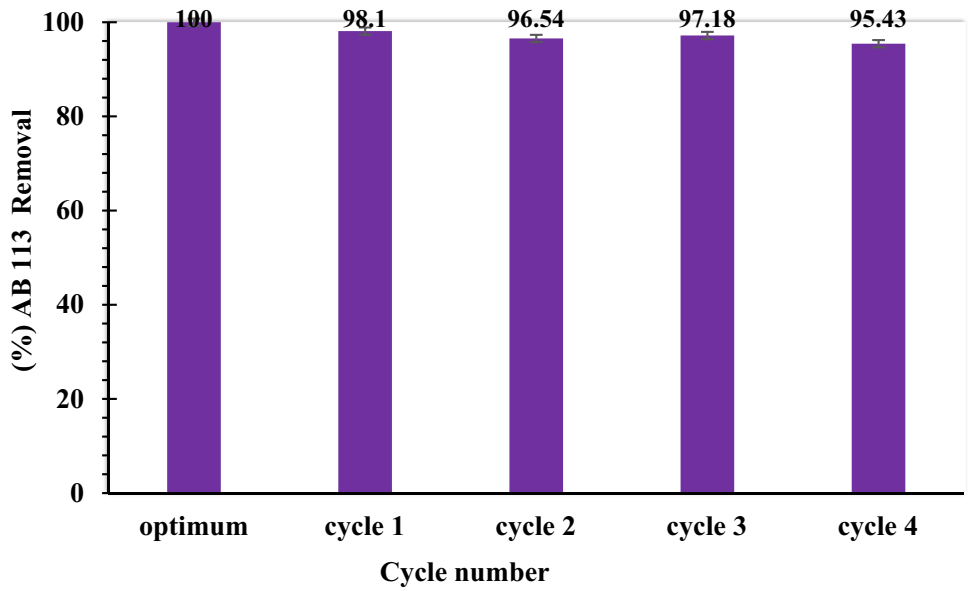

Fig. 10 Recycle efficiency of nZVI

4 Conclusion

This study was performed to optimize the removal of AB 113 dye in the process of zero valent iron nanoparticle/persulfate (nZVI @PS) by using the statistical model of response procedure (RSM) with BBD test design. The results indicated that by increasing the pH and concentration of AB 113, the oxidation efficiency declines so that the pH and the optimal concentration are 3 and 46 mg/L, respectively. Also, the catalyst dose in the values of nZVI = 0.08 and PS = 0.14 g/L has the highest efficiency and by increasing and decreasing the dose of that amount, the efficiency decreases. Time is one of the main parameters in this process, in which the optimal value of oxidation time is 50 min. Under optimal conditions, the process efficiency is 100%. Due to the acceptable performance and proper removal of AB 113 dye, this process can be used as a suitable method and with high efficiency in the treatment of wastewater containing AB 113 dye. Also, according to the Pareto diagram, the greatest effect on the removal of AB 113 was related to the pH variable.

Author contribution YP participated in the conceptualization and design of the research and supervised the work. PP, AA, and AB are responsible for experimental analysis and interpretation of data. SAM and YR contributed to literature search and quality assessment. All authors have read and approved the final paper as submitted.

Funding This research was financially supported by the honorable deputy of Research and Technology of Ardabil University of Medical Sciences and Health Services (with project code of IR.ARUMS.REC.1398.223).

Declarations

Conflicts of interest The authors declare no competing interests.

References

1. Gong J-L, Wang B, Zeng G-M, Yang C-P et al (2009) Removal of cationic dyes from aqueous solution using magnetic multi-wall carbon nanotube nanocomposite as adsorbent. J Hazard Mater 164(2–3):1517–1522
2. Khosravi R, Hazrati S, Fazlzadeh M (2016) Decolorization of AR18 dye solution by electrocoagulation: sludge production and electrode loss in different current densities. Desalin Water Treat 57(31):14656–14664
3. Chatterjee S, Chatterjee T, Woo SH (2011) Influence of the polyethyleneimine grafting on the adsorption capacity of chitosan beads for Reactive Black 5 from aqueous solutions. Chem Eng J 166(1):168–175
4. Aguilar ZG, Brillas E, Salazar M, Nava JL et al (2017) Evidence of Fenton-like reaction with active chlorine during the electrocatalytic oxidation of acid yellow 36 azo dye with Ir-Sn-Sb oxide anode in the presence of iron ion. Appl Catal B 206:44–52
5. Rahmani AR, Shabanloo A, Fazlzadeh M, Poureshgh Y (2016) Investigation of operational parameters influencing in treatment of dye from water by electro-Fenton process. Desalin Water Treat 57(51):24387–24394
6. Gupta V, Gupta B, Rastogi A, Agarwal S et al (2011) A comparative investigation on adsorption performances of mesoporous activated carbon prepared from waste rubber tire and activated carbon for a hazardous azo dye—acid blue 113. J Hazard Mater 186(1):891–901
7. Leodopoulos C, Doulia D, Gimouhopoulos K (2015) Adsorption of cationic dyes onto bentonite. Sep Purif Rev 44(1):74–107
8. Amin NK (2009) Removal of direct blue-106 dye from aqueous solution using new activated carbons developed from pomegranate peel: adsorption equilibrium and kinetics. J Hazard Mater 165(1–3):52–62
9. Iram M, Guo C, Guan Y, Ishfaq A et al (2010) Adsorption and magnetic removal of neutral red dye from aqueous solution using Fe_3O_4 hollow nanospheres. J Hazard Mater 181(1–3):1039–1050
10. Moussavi G, Mahmoudi M (2009) Removal of azo and anthraquinone reactive dyes from industrial wastewaters using MgO nanoparticles. J Hazard Mater 168(2–3):806–812
11. Mahvi A, Ghanbarian M, Nasseri S, Khairi A (2009) Mineralization and discoloration of textile wastewater by TiO2 nanoparticles. Desalination 239(1–3):309–316
12. Jeni J, Kanmani S (2011) Solar nanophotocatalytic decolorisation of reactive dyes using titanium dioxide. J Environ Health Sci Eng 8(1):15–24
13. Fang G, Li J, Zhang C, Qin F et al (2022) Periodate activated by manganese oxide/biochar composites for antibiotic degradation in aqueous system: combined effects of active manganese species and biochar. Environ Pollut 300:118939
14. Parastar S, Nasseri S, Borji SH, Fazlzadeh M et al (2013) Application of Ag-doped TiO_2 nanoparticle prepared by photodeposition method for nitrate photocatalytic removal from aqueous solutions. Desalin Water Treat 51(37–39):7137–7144
15. Ferreira SC, Bruns R, Ferreira H, Matos G et al (2007) Box-Behnken design: an alternative for the optimization of analytical methods. Anal Chim Acta 597(2):179–186
16. Block PA, Brown RA, Robinson D (2004) Novel activation technologies for sodium persulfate in situ chemical oxidation. in Proceedings of the Fourth International Conference on the remediation of chlorinated and recalcitrant compounds. Battelle Press, Columbus
17. Lin H, Wu J, Zhang H (2013) Degradation of bisphenol A in aqueous solution by a novel electro/Fe^{3+}/peroxydisulfate process. Sep Purif Technol 117:18–23
18. Zhou L, Zheng W, Ji Y, Zhang J et al (2013) Ferrous-activated persulfate oxidation of arsenic (III) and diuron in aquatic system. J Hazard Mater 263:422–430
19. Hussain I, Zhang Y, Huang S, Du X (2012) Degradation of p-chloroaniline by persulfate activated with zero-valent iron. Chem Eng J 203:269–276
20. Fang G-D, Dionysiou DD, Wang Y, Al-Abed SR et al (2012) Sulfate radical-based degradation of polychlorinated biphenyls: effects of chloride ion and reaction kinetics. J Hazard Mater 227:394–401
21. Ahmad M, Teel AL, Watts RJ (2013) Mechanism of persulfate activation by phenols. Environ Sci Technol 47(11):5864–5871
22. Oh S-Y, Kang S-G, Chiu PC (2010) Degradation of 2, 4-dinitrotoluene by persulfate activated with zero-valent iron. Sci Total Environ 408(16):3464–3468
23. Oh S-Y, Kang S-G, Kim D-W, Chiu PC (2011) Degradation of 2, 4-dinitrotoluene by persulfate activated with iron sulfides. Chem Eng J 172(2–3):641–646

24. Eberle DE (2015) ISCO of volatile organic contaminants using peroxone activated persulfate and cyclodextrin. University of Rhode Island
25. Soubh AM, Abdoli MA, Ahmad LA (2021) Optimizing the removal of methylene blue from aqueous solutions using persulfate activated with nanoscale zero valent iron (nZVI) supported by reduced expanded graphene oxide (rEGO). Environ Health Eng Manag 8(1):15–24
26. Cojocaru C, Zakrzewska-Trznadel G (2007) Response surface modeling and optimization of copper removal from aqua solutions using polymer assisted ultrafiltration. J Membr Sci 298(1–2):56–70
27. Montgomery DC (2017) Design and analysis of experiments. Wiley
28. Clarke GM (1997) Introduction to the Design and Analysis of Experiments. Arnold
29. Shokoohi R, Samadi MT, Amani M, Poureshgh Y (2018) Modeling and optimization of removal of cefalexin from aquatic solutions by enzymatic oxidation using experimental design. Braz J Chem Eng 35:943–956
30. Sh A, Haghighi M, Rashtbari Y, Mokhtari S (2019) Optimization of acid blue 113 adsorption from aqueous solutions by natural bentonite using response surface model: isotherm and kinetic study. Journal of Health 10(3):287–301
31. Box GE, Behnken DW (1960) Some new three level designs for the study of quantitative variables. Technometrics 2(4):455–475
32. Shokoohi R, Samadi MT, Amani M, Poureshgh Y (2018) Optimizing laccase-mediated amoxicillin removal by the use of box–behnken design in an aqueous solution. Desalin Water Treat 119:53–63
33. Pourali P, Behzad M, Arfaeinia H, Ahmadfazeli A et al (2021) Removal of acid blue 113 from aqueous solutions using low-cost adsorbent: adsorption isotherms, thermodynamics, kinetics and regeneration studies. Sep Sci Technol 56(18):3079–3091
34. Rashtbari Y, Sher F, Afshin S, Hamzezadeh A et al (2022) Green synthesis of zero-valent iron nanoparticles and loading effect on activated carbon for furfural adsorption. Chemosphere 287:132114
35. Rashtbari Y, Américo-Pinheiro JHP, Bahrami S, Fazlzadeh M et al (2020) Efficiency of zeolite coated with zero-valent iron nanoparticles for removal of humic acid from aqueous solutions. Water Air Soil Pollut 231(10):1–15
36. Afshin S, Rashtbari Y, Ramavandi B, Fazlzadeh M et al (2020) Magnetic nanocomposite of filamentous algae activated carbon for efficient elimination of cephalexin from aqueous media. Korean J Chem Eng 37(1):80–92
37. Abdollahzadeh H, Fazlzadeh M, Afshin S, Arfaeinia H, Feizizadeh A, Poureshgh Y et al (2022) Efficiency of activated carbon prepared from scrap tires magnetized by Fe3O4 nanoparticles: characterisation and its application for removal of reactive blue19 from aquatic solutions. Int J Environ Anal Chem 102(8):1911–1925
38. Khosravi R, Eslami H, Zarei A, Heidari M et al (2018) Comparative evaluation of nitrate adsorption from aqueous solutions using green and red local montmorillonite adsorbents. Desalination Water Treat 116:119–128
39. Chen Z-B, Cui M-H, Ren N-Q, Chen Z-Q et al (2011) Improving the simultaneous removal efficiency of COD and color in a combined HABMR–CFASR system based MPDW. Part 1: Optimization of operational parameters for HABMR by using response surface methodology. Bioresour Technol 102(19):8839–8847
40. Wu J, Zhang H, Oturan N, Wang Y et al (2012) Application of response surface methodology to the removal of the antibiotic tetracycline by electrochemical process using carbon-felt cathode and DSA (Ti/RuO_2–IrO_2) anode. Chemosphere 87(6):614–620
41. Khajeh M (2009) Optimization of microwave-assisted extraction procedure for zinc and copper determination in food samples by Box-Behnken design. J Food Compos Anal 22(4):343–346
42. Khajeh M (2011) Optimization of process variables for essential oil components from Satureja hortensis by supercritical fluid extraction using Box-Behnken experimental design. The Journal of Supercritical Fluids 55(3):944–948
43. Khosravi R, Fazlzadehdavil M, Barikbin B, Hossini H (2015) Electro-decolorization of reactive red 198 from aqueous solutions using aluminum electrodes systems: modeling and optimization of operating parameters. Desalin Water Treat 54(11):3152–3160
44. WEF AA (2005) Standard methods for the examination of waterand wastewater. American Public Health Association, AmericanWater Works Association, Water Environmental Federation, 21st Edition, Washington DC, USA
45. Ray A, Gupta SD (2013) A panoptic study of antioxidant potential of foliar gel at different harvesting regimens of Aloe vera L. Ind Crops Prod 51:130–137
46. Fazlzadeh M, Rahmani K, Zarei A, Abdoallahzadeh H et al (2017) A novel green synthesis of zero valent iron nanoparticles (NZVI) using three plant extracts and their efficient application for removal of Cr (VI) from aqueous solutions. Adv Powder Technol 28(1):122–130
47. Kumar H, Rani R (2013) Structural and optical characterization of ZnO nanoparticles synthesized by microemulsion route. Int Lett Chem Phys Astron 19:26–36
48. Weng X, Huang L, Chen Z, Megharaj M et al (2013) Synthesis of iron-based nanoparticles by green tea extract and their degradation of malachite. Ind Crops Prod 51:342–347
49. Jiang Y, Luo Y, Zhang F, Guo L et al (2013) Equilibrium and kinetic studies of CI Basic Blue 41 adsorption onto N, F-codoped flower-like TiO_2 microspheres. Appl Surf Sci 273:448–456
50. Chieng HI, Lim LB, Priyantha N (2015) Enhancing adsorption capacity of toxic malachite green dye through chemically modified breadnut peel: equilibrium, thermodynamics, kinetics and regeneration studies. Environ Technol 36(1):86–97
51. Pavan FA, Camacho ES, Lima EC, Dotto GL et al (2014) Formosa papaya seed powder (FPSP): preparation, characterization and application as an alternative adsorbent for the removal of crystal violet from aqueous phase. J Environ Chem Eng 2(1):230–238
52. Leili M, Fazlzadeh M, Bhatnagar A (2018) Green synthesis of nano-zero-valent iron from nettle and thyme leaf extracts and their application for the removal of cephalexin antibiotic from aqueous solutions. Environ Technol 39(9):1158–1172
53. Huang L, Zhou S, Jin F, Huang J et al (2014) Characterization and mechanism analysis of activated carbon fiber felt-stabilized nanoscale zero-valent iron for the removal of Cr (VI) from aqueous solution. Colloids Surf, A 447:59–66
54. Sangeetha G, Rajeshwari S, Venckatesh R (2011) Green synthesis of zinc oxide nanoparticles by aloe barbadensis miller leaf extract: structure and optical properties. Mater Res Bull 46(12):2560–2566
55. Rahmani AR, Ghafari HR, Samadi MT, Zarabi M (2011) Synthesis of zero valent iron nanoparticles (nzvi) and its efficiency in arsenic removal from aqueous solutions. Water Wastewater 1:35–41
56. Hoseinzadeh E, Rezaee A, Shams Khorramabadi G, Azizi S et al (2014) Evaluation of photocatalytic convertion of hexavalent chromium (Cr (VI)) to trivalent chromium (Cr (III)) in the presence of zinc oxide nanoparticle from aqueous solution. J Mazandaran Univ Med Sci 23(1):116–132
57. Huang J, Yi S, Zheng C, Lo IM (2019) Persulfate activation by natural zeolite supported nanoscale zero-valent iron for trichloroethylene degradation in groundwater. Sci Total Environ 684:351–359

58. Gojarati SS, Hajisafari M, Khosravirad MM (2020) Study of photocatalytic activity of zinc oxide nanoparticles extracted from leaching residue of zinc melting factory to remove NB21 dye in UV light. J Water Wastewater 31(4):87–98
59. Shabanlo A, Khorshidi M, Seid Mohammadi A (2018) Synergistic effect investigation of persulfate and nano zero-valent iron in degradation of acid blue 113 in the presence of 40 KHz ultrasonic irradiation. J Sabzevar Univ Med Sci 24(6):81–93
60. Ben W, Qiang Z, Pan X, Chen M (2009) Removal of veterinary antibiotics from sequencing batch reactor (SBR) pretreated swine wastewater by Fenton's reagent. Water Res 43(17):4392–4402
61. Shu H-Y, Chang M-C, Chen C-C, Chen P-E (2010) Using resin supported nano zero-valent iron particles for decoloration of acid blue 113 azo dye solution. J Hazard Mater 184(1–3):499–505
62. Xu X-R, Li X-Z (2010) Degradation of azo dye Orange G in aqueous solutions by persulfate with ferrous ion. Sep Purif Technol 72(1):105–111
63. Masomboon N, Ratanatamskul C, Lu M-C (2010) Chemical oxidation of 2, 6-dimethylaniline by electrochemically generated Fenton's reagent. J Hazard Mater 176(1–3):92–98
64. Gayathri P, Yesodharan S, Yesodharan E (2019) Microwave/persulphate assisted ZnO mediated photocatalysis (MW/PS/UV/ZnO) as an efficient advanced oxidation process for the removal of RhB dye pollutant from water. J Environ Chem Eng 7(4):103122
65. Zhao YS, Sun C, Sun JQ, Zhou R (2015) Kinetic modeling and efficiency of sulfate radical-based oxidation to remove p-nitroaniline from wastewater by persulfate/Fe_3O_4 nanoparticles process. Sep Purif Technol 142:182–188
66. Liang C, Wang Z-S, Bruell CJ (2007) Influence of pH on persulfate oxidation of TCE at ambient temperatures. Chemosphere 66(1):106–113
67. Yang S, Yang X, Shao X, Niu R et al (2011) Activated carbon catalyzed persulfate oxidation of Azo dye acid orange 7 at ambient temperature. J Hazard Mater 186(1):659–666
68. Shokoohi R, Salari M, Shabanloo A, Shabanloo N et al (2020) Catalytic activation of persulphate with Mn_3O_4 nanoparticles for degradation of acid blue 113: process optimisation and degradation pathway. Int J Environ Anal Chem 1–20. https://doi.org/10.1080/03067319.2020.1773810
69. Wang K-S, Lin C-L, Wei M-C, Liang H-H et al (2010) Effects of dissolved oxygen on dye removal by zero-valent iron. J Hazard Mater 182(1–3):886–895
70. Talebi S, ChaibakhshLangroudi N, Moradi-Shoeili Z (2017) Optimization of photodegradation of acid blue 113 dye on anatase TiO_2 nanocatalyst using response Surface methodology. J Environ Health Eng 4(2):149–160
71. Souri Z, Ansari A, Nematollahi D, Mazloum-Ardakani M (2020) Electrocatalytic degradation of dibenzoazepine drugs by fluorine doped β-PbO_2 electrode: new insight into the electrochemical oxidation and mineralization mechanisms. J Electroanal Chem 862:114037
72. Samarghandi MR, Tari K, Shabanloo A, Salari M et al (2020) Synergistic degradation of acid blue 113 dye in a thermally activated persulfate (TAP)/ZnO-GAC oxidation system: degradation pathway and application for real textile wastewater. Sep Purif Technol 247:116931
73. Dargahi A, Ansari A, Nematollahi D, Asgari G et al (2019) Parameter optimization and degradation mechanism for electrocatalytic degradation of 2, 4-diclorophenoxyacetic acid (2, 4-D) herbicide by lead dioxide electrodes. RSC Adv 9(9):5064–5075
74. Wu J, Zhang H, Qiu J (2012) Degradation of Acid Orange 7 in aqueous solution by a novel electro/Fe^{2+}/peroxydisulfate process. J Hazard Mater 215:138–145
75. Ponnusami V, Krithika V, Madhuram R, Srivastava S (2007) Biosorption of reactive dye using acid-treated rice husk: factorial design analysis. J Hazard Mater 142(1–2):397–403
76. Li Y, Wang X, Shao J, Li P et al (2016) Utilization of pyrolytic char derived from bamboo chips for furfural removal: kinetics, isotherm, and thermodynamics. Energy Sources Part A Recovery Util Environ Effects 38(11):1520–1529
77. Tarlani Azar M, Leili M, Taherkhani F, Bhatnagar A (2016) A comparative study for the removal of aniline from aqueous solutions using modified bentonite and activated carbon. Desalin Water Treat 57(51):24430–24443
78. Muthirulan P, Meenakshisundararam M, Kannan N (2013) Beneficial role of ZnO photocatalyst supported with porous activated carbon for the mineralization of alizarin cyanin green dye in aqueous solution. J Adv Res 4(6):479–484
79. Dargahi A, Samarghandi MR, Vaziri Y, Ahmadidoost G et al (2019) Kinetic study of the photocatalytic degradation of the acid blue 113 dye in aqueous solutions using zinc oxide nanoparticles immobilized on synthetic activated carbon. J Adv Environ Health Res 7(2):75–85
80. Moussavi G, Khavanin A, Alizadeh R (2009) The investigation of catalytic ozonation and integrated catalytic ozonation/biological processes for the removal of phenol from saline wastewaters. J Hazard Mater 171(1–3):175–181
81. Suárez-Ojeda ME, Carrera J, Metcalfe IS, Font J (2008) Wet air oxidation (WAO) as a precursor to biological treatment of substituted phenols: refractory nature of the WAO intermediates. Chem Eng J 144(2):205–212
82. Soubh AM, Baghdadi M, Abdoli MA, Aminzadeh B (2018) Zero-valent iron nanofibers (ZVINFs) immobilized on the surface of reduced ultra-large graphene oxide (rULGO) as a persulfate activator for treatment of landfill leachate. J Environ Chem Eng 6(5):6568–6579
83. Barzegar G, Jorfi S, Zarezade V, Khatebasreh M et al (2018) 4-Chlorophenol degradation using ultrasound/peroxymonosulfate/nanoscale zero valent iron: reusability, identification of degradation intermediates and potential application for real wastewater. Chemosphere 201:370–379
84. Hu S, Yao H, Wang K, Lu C et al (2015) Intensify removal of nitrobenzene from aqueous solution using nano-zero valent iron/granular activated carbon composite as Fenton-like catalyst. Water Air Soil Pollut 226(5):1–13